



The Evolution and Prevention of Water Inrush Due to Fault Activation at Working Face No. II 632 in the Hengyuan Coal Mine

Yang Hu¹ · Jian Sun² · Weiqun Liu¹ · Dayong Wei³

Received: 17 November 2017 / Accepted: 22 December 2018 / Published online: 3 January 2019
© Springer-Verlag GmbH Germany, part of Springer Nature 2019

Abstract

The water-bearing capacity and abnormal water-bearing area of the coal seam floor of working face no. II 632 at the Hengyuan coal mine was investigated using the network parallel electrical method. Based on the limit equilibrium theory and Mohr–Coulomb yield criterion, we obtained a critical water pressure formula. Using fault DF137 as an example, we found that the abnormal water-bearing phenomena around the working face was related to nearby faults and that the water inrush was mainly due to faults being activated during mining. The pathway of water inrush under the coupled effects of stress induced by mining and the confined water pressure was modelled in Flac3D based on the fluid structure interaction (FSI) method. Considering the economics and operational convenience, grouting the working face floor was recommended to prevent an inrush. Based on a geophysical evaluation, the grouting effectively prevented a potential inrush.

Keywords Confined aquifer · Mechanics modelling · FSI · Fault activation induced by mining · Water inrush

Introduction

Water inrush events can lead to extensive economic losses, hazardous working conditions, and severe pollution of the surrounding environment (Miao 2011). Water inrush is directly related to a mine's fault structures. Faults without water pathways can become activated and transmissive during the coal mining process (Xu et al. 2012). Many studies have focused on the prediction and prevention of inrush events in coal mining (Guo et al. 2017; Hofmann and Scheepers 2011; Hu et al. 2014; Lee et al. 2012; Li et al. 2011, 2013, 2017; Liu et al. 2014; Wu et al. 2017; Zhao et al. 2013; Zhou et al. 2017). Sainoki and Hani (2014)

studied the mechanism of fault activation with Flac3D and found that the maximum increase in relative shear displacement along a fault is directly related to the mining depth and friction angle of the fault, but not with the expansion angle and stiffness of the fault. This scenario provides a basis for mine water inrush from floor strata through faults. Zhang et al. (2014) studied and analysed the mechanism of such inrushes through faults above a confined aquifer, based on simulations, the effects of varying the confined water pressure, permeability, porosity, and other hydrogeological conditions. This report has become an important theoretical reference for researchers who study mining in different geological areas and assess the risk of water inrush via faults. Wang et al. (2017) established a new model for evaluating and predicting water inrush through faults in the Lu-an mining area based on fractal theory. Liu et al. (2017) simulated the process of lagging water inrush from an insidious fault in a coal seam floor and verified the feasibility of applying the approach in mining practice.

We theoretically studied the mechanism of water inrush through activated faults above a confined aquifer and developed a criterion for this water inrush process. In addition, using data from working face no. II 632 of the Hengyuan coal mine in China, we investigated the influence of nearby active faults on water inrush during mining and simulated

Electronic supplementary material The online version of this article (<https://doi.org/10.1007/s10230-018-00579-w>) contains supplementary material, which is available to authorized users.

✉ Yang Hu
hyhyc2012@126.com

- ¹ State Key Laboratory for Geomechanics and Deep Underground Engineering, China University of Mining and Technology, Xuzhou 221116, China
- ² School of Energy and Safety, Anhui University of Science and Technology, Huainan 232001, China
- ³ Hengyuan Coal Mine, Anhui Hengyuan Coal and Electricity Group Company Limited, Huaibei 235163, China

the inrush pathways. Corresponding preventive measures were then proposed.

Study of the Conditions of Working Face No. II 632

Conditions of the Mine Wells and Working Faces

Located in Huaibei, Anhui Province (Fig. 1), the Hengyuan coal mine is managed by the Hengyuan Coal-Electricity Group Company. It is a part of the Suixiao mining district in the Huaibei coalfield. The main minable coal seams in the mine are seam numbers four and six; the authorized productive capacity is 200 Mt/a. There are two production levels: level one with a standard elevation of -400 m and level two, with a standard elevation of -600 m. Working face no. II 632, located at the top of the mining area, is the first working face of the no. 63 mining area of the second production level, and was mined along the strike using long-wall mining.

Hydrogeological Conditions at the Working Face

The details of the lithology of the roof and floor of the working face, based on prospecting and drilling data, are shown in Fig. 2. Previous research and investigations identified 21 faults connected by 21 fault points during tunneling. The details of these faults are shown in supplemental







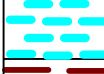

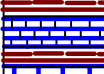



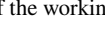
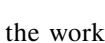
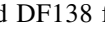

Chronostratigraphic Unit		Column	Thickness(m)	Lithology
System	Formation			
Permian	Shanxi Formation		23.6	Siltstone
			6.5	Mudstone
			4.5	Siltstone
			3.6	Fine sandstone
			3.13	Mudstone
			2.8	Coal Seam
			11.6	sandstone
			21.3	Siltstone
Carboniferous	Taiyuan Formation		11.3	Marine mudstone
			2.2	Limestone(L1)
			4.8	Mudstone
			3.3	Limestone(L2)
			1.7	Mudstone
			5.5	Limestone(L3)
			1.9	Mudstone
			10	Limestone(L4)

Fig. 2 Borehole histogram of the working face

Table S-1. In addition, the working face no. II 632 also includes the DF137 and DF138 faults. The former has a

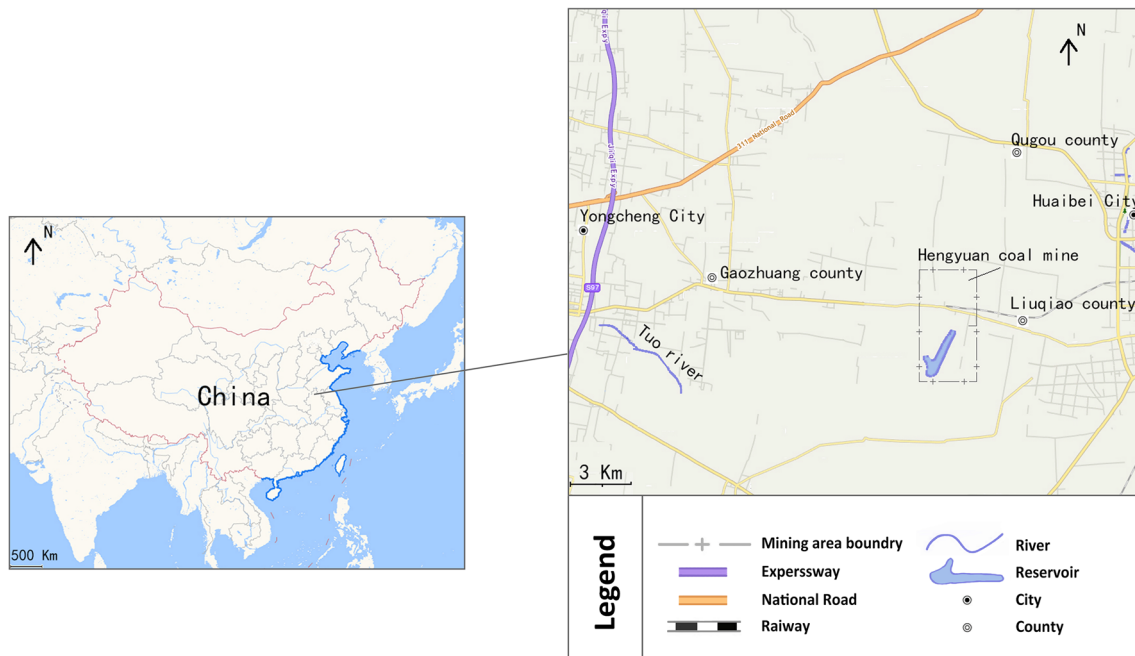


Fig. 1 The location of Huaibei city (Hengyuan coal mine) in China

4 m throw and a dip angle of 50°, while the latter has a 3 m throw and a dip angle of 45°. The potential source of water inrush mainly comes from the limestone water in the Taiyuan Formation below the working face. The Taiyuan Formation is 115.55 m thick and consists of limestone and thin mudstone. Limestone comprises 46.6% of the strata. The formation has 13 layers, labelled L_1 to L_{13} , from top to bottom. The L_3 , L_4 , L_5 , L_{12} , and L_{13} layers are relatively thick, while the other layers are relatively thin. So far, only layers L_1 – L_4 have been explored. Based on drilling data, the limestone deposits in layers L_1 – L_4 contain much stored water and include many micro-cracks in the karst. Such cracks could significantly affect mining and create hazards. In addition, based on an outflow test, the permeability of the limestone in L_3 is high. In the middle of the no. II 632 working face, the average distance between the no. 6 coal seam and the top of the L_1 limestone layer is 46 m. According to hydrological data from the observation hole and the water table contour map of the limestone aquifer, it can be inferred that the water pressure in the limestone aquiclude at the top of L_1 is 4.14–5.16 MPa. Note that the regulation for coal mine water prevention and control in China (SACMSC 2009) defines the floor of a coal seam with a fault or developmental fissure zone as incomplete, and the corresponding empirical threshold of the water inrush coefficient is 0.06 MPa/m. The water inrush coefficient can be expressed as an empirical formula:

$$T_s = \frac{P}{M}, \quad (1)$$

where: T_s = the coefficient of water bursting (MPa/m), P = the water pressure at the coal seam floor (MPa), and M = the thickness of the coal floor aquiclude (m). Thus, the water inrush coefficient in the limestone at the top of

L_4 is between 0.09 and 1.12 MPa/m, which is higher than 0.06 MPa/m (the empirical critical value). Therefore, water inrush is likely to occur during mining at this working face.

Detection on the Water-Bearing Properties at the Working Face

To prevent the underground water from inrushing through the floor or faults during mining, it was necessary to determine the water-bearing properties at the floor of the working face, especially near the known faults. We used the network parallel electrical method. The main types of equipment required include one intrinsically safe network parallel electrical instrument, one industrial computer with a power supply, two cables, and a copper hammer. There were four monitoring stations: two at the air roadway and two at the conveyor roadway. Sixty-four electrodes were arranged at each station, and the distance between adjacent electrodes was 5 m. The layout of a monitoring station is shown in Fig. 3. The horizontal apparent resistivity of the limestone bed was obtained by detection methods at the working floor (Fig. 4).

Figure 4 shows that there are two low-resistivity areas in the limestone bed at working face no. II 632:

1. The #1 low-resistivity area (DZ2) is located near the airway with an abscissa from 40 to 120 m and an ordinate from 10 to 50 m. According to the geology and 3D earthquake research, DZ2 is close to the wing of a synclinal axis where the dip angle of the coal seam is large and part of the seam is thin; therefore, the electrical properties vary between seams. These findings

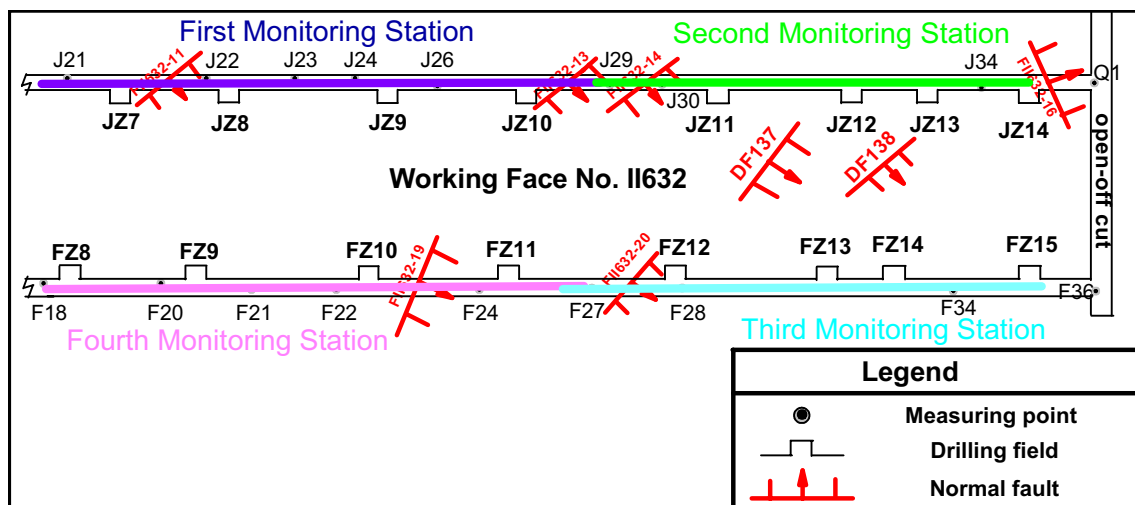


Fig. 3 The layout of the monitoring stations

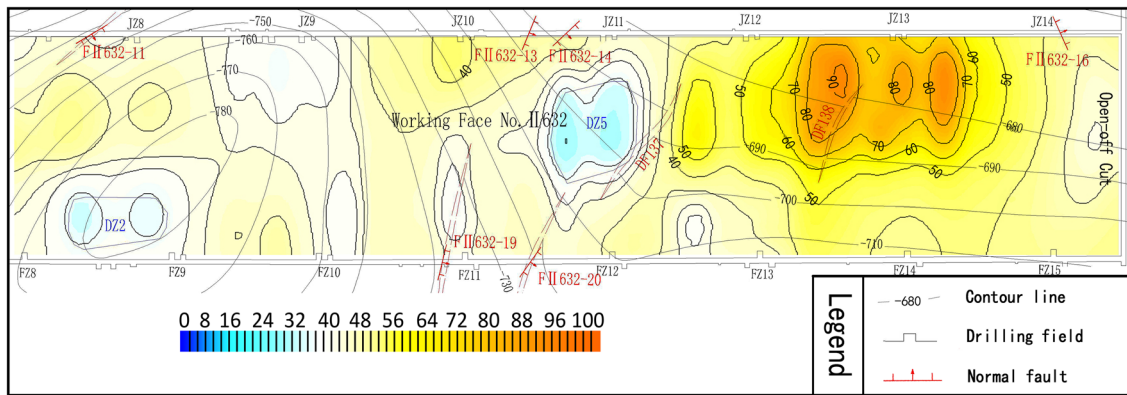


Fig. 4 Horizontal microsection of the apparent resistivity of the limestone section

suggest that the water-bearing property of this area is comparatively weak.

2. The #2 low-resistivity area (DZ5) is near the middle of the working face with an abscissa from 440 to 520 m and an ordinate from 60 to 140 m. Faults FII632-13 and 14 were discovered during mining at the haulage way, and the working face includes the DF137 fault. This discovery of the faults resulted in a larger estimated dip angle of the coal and a thinner predicted coal seam. Thus, the tectonic stress is concentrated in this area, which can have hazardous effects on mining. In addition, the outflow of No. JZ11-3 borehole in the #2 low-resistivity area (DZ5) was 32 m³/h, which exceeds the average borehole outflow. Based on the above analysis, both this area and the region below it were characterized as water bearing.

Theoretical Analysis

According to the results of the network parallel electrical method, faults are exposed and extend downward beneath the working floor. These faults, including DF137, have enabled the working floor to bear water. Therefore, fault DF137 was used to investigate whether water would burst out of the fault under the combined conditions of the confined water pressure and mining actions. In this section, based on the limit equilibrium theory and Mohr–Coulomb theory, we developed formulas for the changes in the critical water pressure during water inrush caused by mining near the faults.

Critical Water Pressure of Water Inrush during Mining near the Faults

In the direction of working face advancement, we take an infinitesimal inverted trapezoid from the slope of the bottom protection layer with an arbitrary thickness dy and establish a rectangular coordinate system (Fig. 5). The distance between the open cut and the fault is L' , the distance from the suspended roof to the goaf is L , the distance from the recompacked goaf area and goaf is L_1 ; and the distance between the working face and fault is L_2 . According to the limit equilibrium theory, before water inrush occurs through the floor of the working face, the stresses in the rock strata at the bottom of the goaf are in equilibrium. This relationship can be formulated as (Sun et al. 2019):

$$\left. \begin{aligned} \sigma_x dy &= \sigma_n \sin \beta \frac{dy}{\sin \beta} + \tau_r \cos \beta \frac{dy}{\sin \beta} \\ \sigma_y l + \tau dy + \tau_r \sin \beta \frac{dy}{\sin \beta} &= (\sigma_y + d\sigma_y) \left(l - \frac{dy}{\tan \beta} \right) + \sigma_n \cos \beta \frac{dy}{\sin \beta} \end{aligned} \right\} \quad (2)$$

where σ_x is the horizontal stress and σ_y is the vertical stress. Based on the Mohr–Coulomb failure criterion, the shear strength of the fault can be calculated as follows:

$$\tau_r = c_r + \sigma_n \tan \varphi_r, \quad (3)$$

where C is the cohesion of the rock mass and φ is the friction angle of the coal seam floor.

In addition, the limit equilibrium condition of rock failure can be expressed as:

$$\sigma_x = \frac{1 - \sin \varphi}{1 + \sin \varphi} \sigma_y - \frac{2C \cos \varphi}{1 + \sin \varphi}. \quad (4)$$

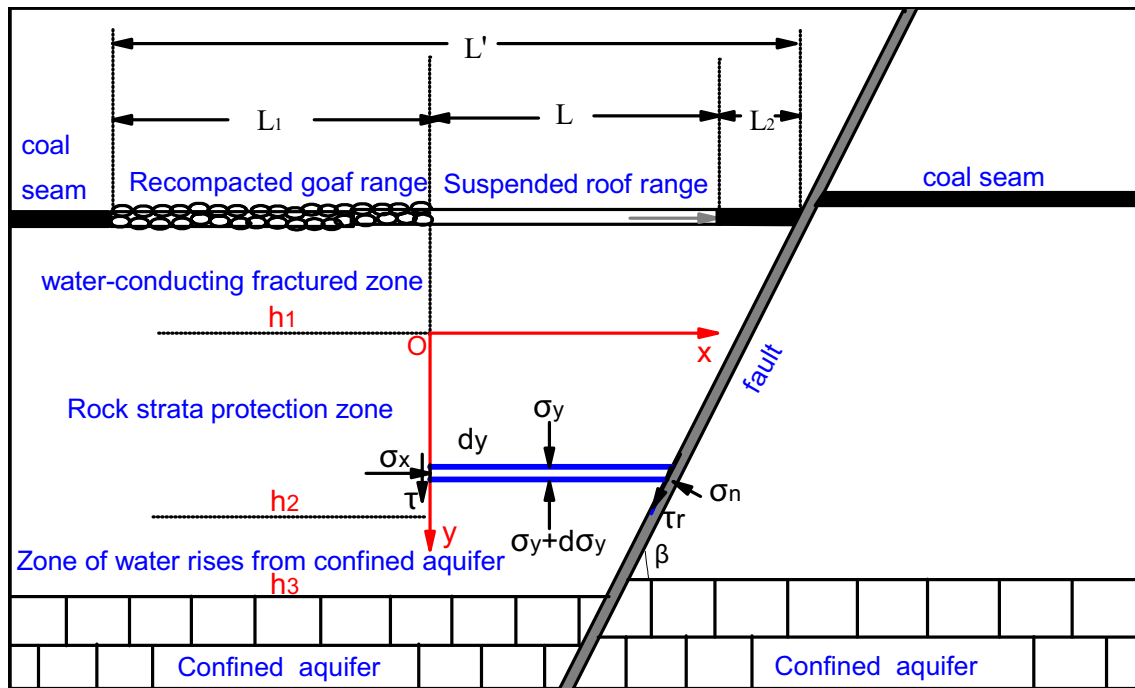


Fig. 5 Mechanical model of water inrush caused by fault activation

Substituting Eqs. (3, 4) and (5) into Eq. (2) yields the following equation.

where B is the integral constant to be determined and D_1 and D_2 are shown in Eq. (9).

$$l d\sigma_y + \left[\frac{(1 - \sin \varphi)(\cot \beta - \tan \varphi_r)}{(1 + \sin \varphi)(1 + \cot \beta \tan \varphi_r)} - \frac{(1 - \sin \varphi)}{1 + \sin \varphi} \tan \varphi - \frac{1}{\tan \beta} \right] \sigma_y d_y - \frac{d_y}{\tan \beta} d\sigma_y - \left\{ \frac{[2C \cos \varphi + C_r(1 + \sin \varphi) \cot \beta](\cot \beta - \tan \varphi_r)}{(1 + \sin \varphi)(1 + \cot \beta \tan \varphi_r)} - \frac{2C \sin \varphi}{1 + \sin \varphi} + C + C_r \right\} d_y = 0. \quad (5)$$

Note that $d\sigma_y d_y$ is omitted because it is a second-order infinitesimal value. Additionally, Eq. (6) can be further simplified to the following form:

$$\frac{d\sigma_y}{d_y} + \left[\frac{(1 - \sin \varphi)(\cot \beta - \tan \varphi_r)}{(1 + \sin \varphi)(1 + \cot \beta \tan \varphi_r)} - \frac{(1 - \sin \varphi) \tan \varphi}{1 + \sin \varphi} - \frac{1}{\tan \beta} \right] \frac{\sigma_y}{l} - \left\{ \frac{[2C \cos \varphi + C_r(1 + \sin \varphi) \cot \beta](\cot \beta - \tan \varphi_r)}{(1 + \sin \varphi)(1 + \cot \beta \tan \varphi_r)} - \frac{2C \sin \varphi}{1 + \sin \varphi} + C + C_r \right\} \frac{1}{l} = 0. \quad (6)$$

After integrating Eq. (6), we obtain the following equations:

$$\begin{cases} \frac{d\sigma_y}{d_y} + \frac{D_1}{l} \sigma_y - \frac{D_2}{l} = 0 \\ \sigma_y = B e^{-\frac{D_1}{l} y} + \frac{D_2}{D_1} \end{cases}, \quad (7)$$

$$\begin{cases} D_1 = \frac{(1 - \sin \varphi)(\cot \beta - \tan \varphi_r)}{(1 + \sin \varphi)(1 + \cot \beta \tan \varphi_r)} - \frac{(1 - \sin \varphi) \tan \varphi}{1 + \sin \varphi} - \frac{1}{\tan \beta}, \\ D_2 = \frac{[2C \cos \varphi + C_r(1 + \sin \varphi) \cot \beta](\cot \beta - \tan \varphi_r)}{(1 + \sin \varphi)(1 + \cot \beta \tan \varphi_r)} - \frac{2C \sin \varphi}{1 + \sin \varphi} + C + C_r, \end{cases} \quad (8)$$

If $y=0$, $\sigma_y = \gamma_1 h_1$ (h_1 : the height of the water-conductive failure zone; γ_1 : the average volume weight). In these cases, $B = \gamma_1 h_1 - D_2/D_1$. If $y=h_2$, then $\sigma_y = P_c - (\gamma_1 h_1 + \gamma_2 h_2)$ (where P_c : progressive upward hydraulic pressure of the confined water. In these cases, $P_c = (\gamma_1 h_1 - D_2/D_1) \exp(-D_1 h_2/l) + D_2/D_1 + (\gamma_1 h_1 + \gamma_2 h_2)$).

Based on the method presented by Yin and Hu (2008), we find that a certain volume of water loss occurs during the upward lifting of confined water. The water loss η is closely related to the permeability k of the rock strata in the coal seam floor and decreases with increasing permeability (k). This relation can be described as $\eta = 0.0906 \exp(-14.969 k)$. Noting that $P_c = P_0 - h_3 \eta$ (P_0 : water pressure of the confined aquifer; h_3 : the height of water rise from the confined aquifer), the maximum pressure from the confined aquifer that the rock strata in the coal seam floor can withstand after fault activation can be calculated as:

$$P_m = \left(\gamma_1 h_1 - \frac{D_2}{D_1} \right) e^{-\frac{D_1}{l} h_2} + \frac{D_2}{D_1} + (\gamma_1 h_1 + \gamma_2 h_2) + h_3 \eta. \quad (9)$$

According to this calculation, under the coupled pressure of the confined water and that induced by mining, the rock strata under the working floor would remain stable even though the fault has been activated and water would not burst from the fault if P_m is greater than P_0 . If P_m is

equal to P_0 , the rock strata under the floor would reach a critical state, and the potential for water outburst would be high.

Calculations Based on the Experimental Results

Based on the above approach, we obtained the following data for fault DF137, and hobble drilling: $H=4$ m, $\beta=50^\circ$, $C=0.5$ MPa, $\varphi=25^\circ$, $C_r=0.04$ MPa, $\varphi_r=15^\circ$, $L=35$ m, $h_1=15$ m, $h_2=25$ m, $h_3=10$ m, $\gamma_1=25$ kN/m³, $\gamma_2=28$ kN/m³, and $\eta=0.073$ MPa/m. After inserting these values into Eq. (9), we obtain $P_m=3.6$ MPa. This indicates that the critical water pressure leading to water inrush is 3.6 MPa. Thus, fault DF137 will cause water inrush events during mining.

Numerical Simulation of the Water Inrush Caused by Fault Activation

Boundary Conditions

To investigate the process of water inrush and the associated flow paths, we used the fluid structure interaction (FSI) Method in Flac3D and established a numerical simulation model (Fig. 6) based on a conceptual geological engineering model (Supplemental Fig. S-1). The length, width, and height of the numerical simulation model were 200, 100, and

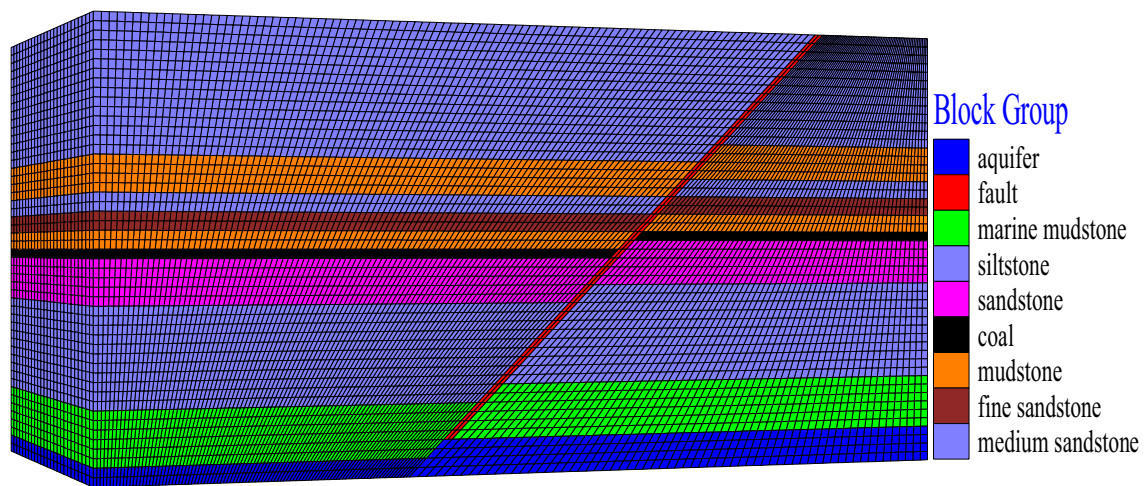


Fig. 6 Numerical simulation model

Table 1 Physical and mechanical parameters of the strata and fault

Lithology	Density (ρ / kgm^{-3})	Bulk modulus (k/GPa)	Shear modulus (G/GPa)	Tension (σ /MPa)	Cohesion (C/MPa)	Friction (Φ /°)	Permeability (K/ms $^{-1}$)	Porosity (η)
Aquifer	3000	21.55	13.52	4.60	5.50	42	1e – 16	0.10
Marine mudstone	2700	14.13	10.16	1.10	5.50	36	1e – 15	0.12
Siltstone	2750	14.78	11.63	2.20	6.50	36	0.8e – 19	0.01
Sandstone	2400	21.04	13.52	1.20	4.90	40	0.9e – 19	0.01
Coal seam	1500	4.97	2.01	0.60	0.80	28	1e – 19	0.01
Mudstone	2500	12.21	9.23	2.25	3.50	40	1.2e – 19	0.02
Fine sandstone	2650	14.01	10.16	3.50	6.10	35	1e – 20	0.01
Medium sandstone	2700	13.68	10.02	2.10	5.50	34	1e – 19	0.02
Mudstone	2550	12.23	9.19	2.35	3.90	40	1.2e – 19	0.02
Siltstone	2700	14.03	11.16	2.25	5.50	36	0.8e – 19	0.02
Fault	2000	2.50	1.20	0.50	0.80	28	1e – 13	0.30

100 m, respectively. The thickness of the coal seam was set to 2 m. The thickness of the confined water located layer in the upper wall of the fault was set to 4 m and the thickness of the confined water layer located in the footwall of the fault was set to 8 m. The X-velocity was set to zero at both the left and right boundaries, and the Y-velocity was set to zero at both the front and rear boundaries. The top boundary was defined as a free surface with a vertical stress. The average density of the strata was 2500 kg/m³, and the equivalent bearing load was 15 MPa. The water pressure on the confined aquifer was set to 5 MPa, and the deformation failure conditions meet the Mohr–Coulomb criterion. The physical and mechanical parameters of the roof, floor strata, and fault are shown in Table 1.

Simulation Results

We adopted a step-by-step excavation method in this model. In each step, the excavation distance was 15 m, and there were 5 steps in total. The distance from the open cut to the left boundary was 20 m. We do not conduct fluid calculations initially. After the initial stress reaches equilibrium, we calculate the FSI during mining.

As shown in Fig. 7, the shear stress around the working face varies with the distance between the working face and the fault. The fault becomes more vulnerable to damage as the mining process approaches it, and the existence of faults in the strata may stop the stresses from penetrating. During mining, the shear stress at the bottom of the fault strata rapidly increases. In addition, the maximum shear stress continuously increases while extraction proceeds at the working face. When the distance is 75, 60, 45, 30, and 15 m, the maximal shear stress at the fault strata is 5.7, 6.9, 7.5, 7.8, and 8.0 MPa, respectively.

As shown in Fig. 7, as the working face advances, the height of the confined water in the fault increases as the

mining distance increases. When the distance between the working face and the fault is 75, 60, 45, 30, and 15 m, the height of the confined water in the fault is 6, 12, 16, 20 and 26 m, respectively. The graph of the seepage vector shows that when the distance between the working face and fault is 15 m, the seepage vector field changes from the bottom to the top of the fault and then reaches the working floor, activating the fault and causing the water inrush.

It can be concluded that as the distance decreases, the fault strata gradually lose stability. Once the stability decreases to the point that the fault is activated, the possibility of water inrush increases. As the distance approaches 15 m, the area of maximal shear stress at the working floor connects to the areas of maximal shear stress in the fault strata, and the risk of fault activation considerably increases.

Prevention of and Solutions for Water Inrush Caused by Fault Activation During Coal Mining

Grouting the Working Floor

Based on the simulation results, the confined water under the floor will flow through the faults and reach the area directly below the working floor. If no action is taken, the water could eventually rush into the working face. To prevent water inrush, we assessed the choice of grouting the working floor, since grouting would reinforce the strata and strengthen the seam.

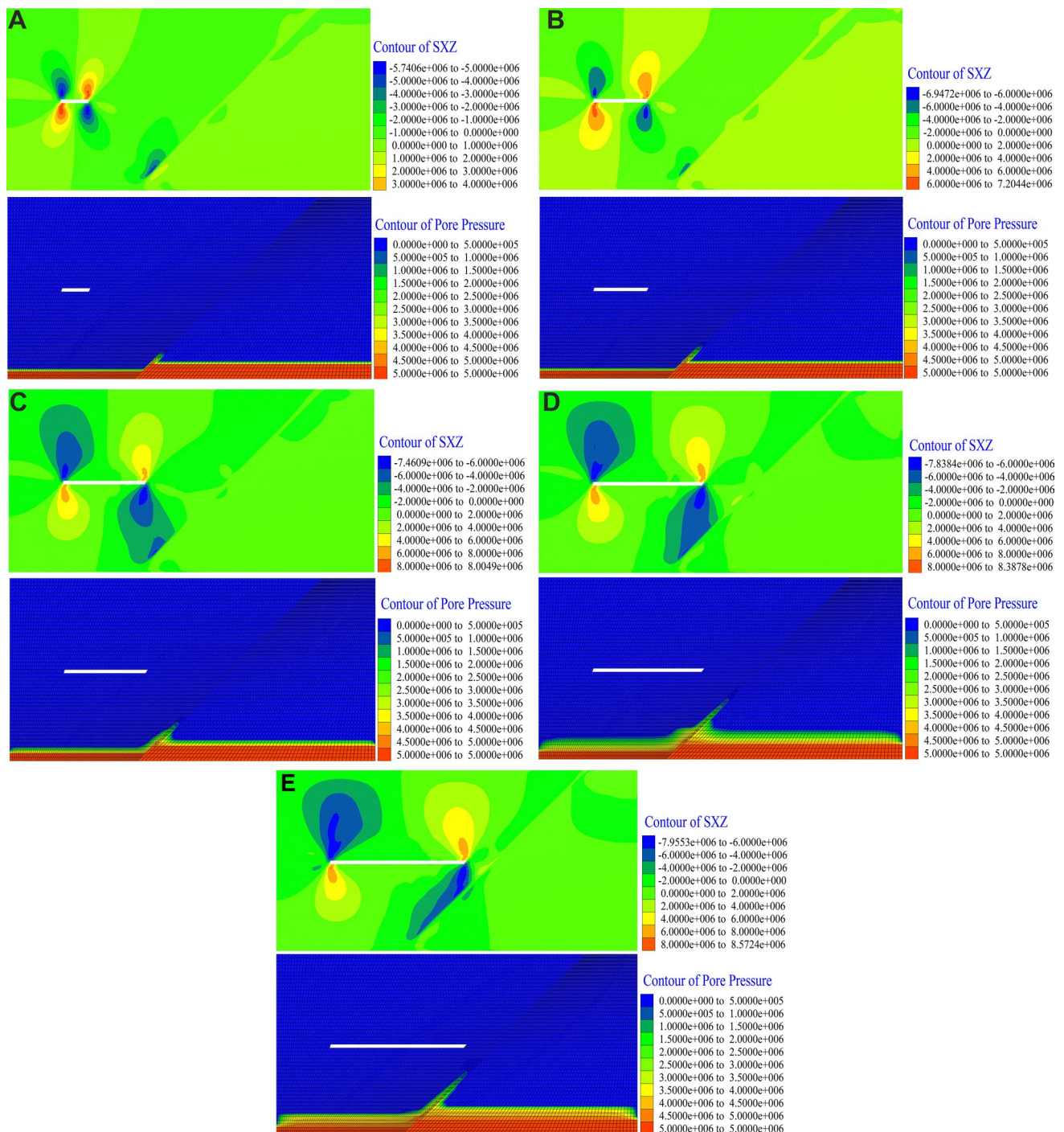


Fig. 7 a–e Nephograms of shear stress and pore pressure at different distances from the working face to the fault

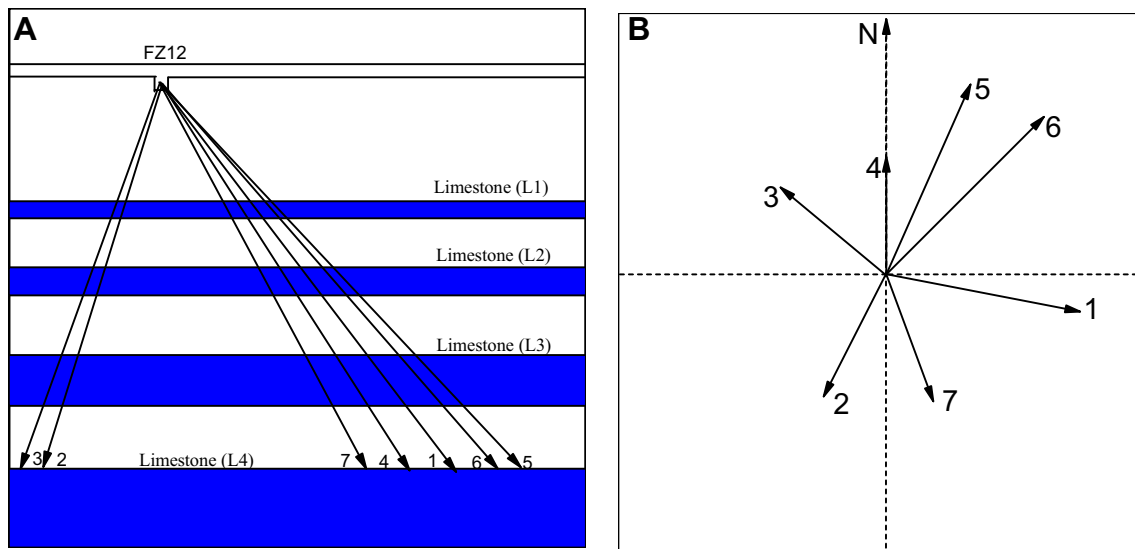
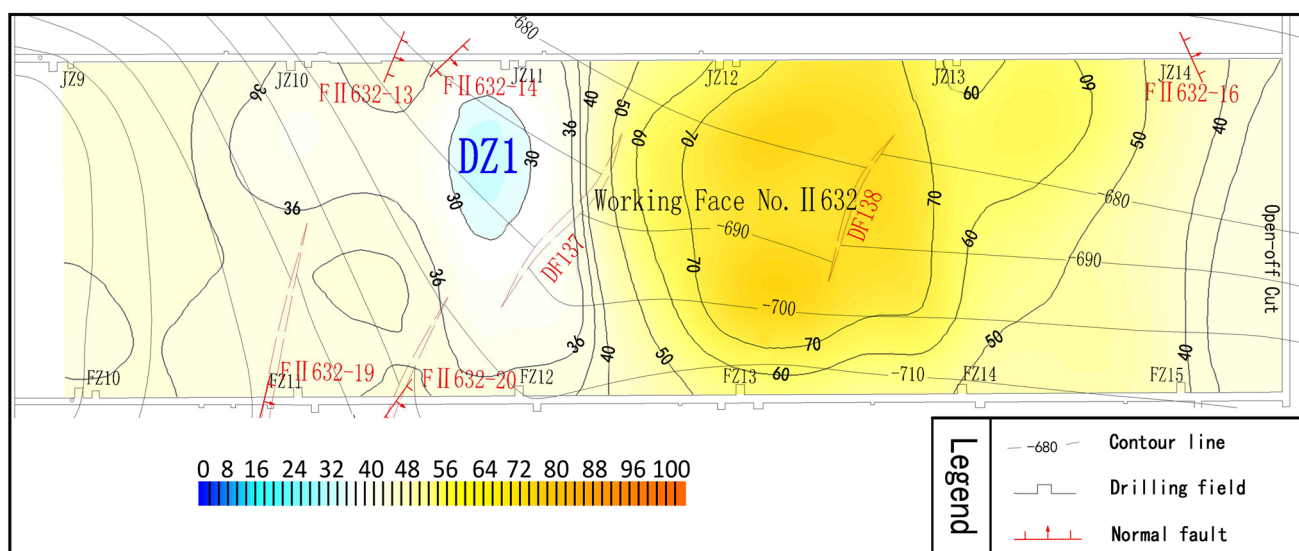
Grouting Methods and Materials Used

We suggested two methods of grouting: orifice closed grouting and sectional downward grouting under static pressure. First, we drilled a hole with a diameter of 153 mm and inserted a 2 m long borehole orifice-pipe with a diameter of 146 mm into the hole. Second, we grouted the borehole

orifice-pipe and waited 48 h until the grout solidified. Third, we continued drilling using a drill with a diameter of 91 mm, 2 m deeper than the no. 2 borehole orifice-pipe we designed. Finally, we continued drilling to the bottom of this hole using a drill with a diameter of 133 mm. We then inserted an orifice pipe that was at least 20 m long with a diameter of 108 mm.

Table 2 The location information and the amount of grout

Serial number	Drilling number	Drilling azimuth (°)	Dip angle (°)	Drilling depth (m)	Final hole location	Grouting amount (m ³)
1	FZ12-1	94	− 56	96	Limestone (L ₄)	27.4
2	FZ12-2	208	− 76	82	Limestone (L ₄)	170.2
3	FZ12-3	287	− 61	92.5	Limestone (L ₄)	1.8
4	FZ12-4	0	− 66	89.5	Limestone (L ₄)	261.4
5	FZ12-5	13	− 46	125	Limestone (L ₄)	91.4
6	FZ12-6	42	− 48	103	Limestone (L ₄)	193.9
7	FZ12-7	173	− 73	82.5	Limestone (L ₄)	1.9


Fig. 8 a, b Schematic drawings of drill holes

Fig. 9 Horizontal microsection of the apparent resistivity in the limestone layer after grouting

The grouting was conducted using 32.5 composite silicate cement; the daily maximum amount used was as high as 1000 tons. The water used met national standards, and the hourly maximum volume of water used was as much as 100 m³. The grouting proceeded in two phases, filling of the openings and then grouting at stable pressure. After the second phase, the rate of grouting was gradually decreased, until it reached 60 L/min. This rate was maintained for \approx 30 min, at which point the standard grouting process was complete.

There were 7 points to grout on the working floor located in the middle of the airway of working face no. II 632. The location information and the amount of grout are given in Table 2, and the schematic drawings of drill holes are shown in Fig. 8. The site conditions for grouting at the no. II 632 working face are shown in Supplemental Figure S-2.

Geophysical Exploration

To evaluate the effect of the grouting, we re-evaluated the working floor using the network parallel electrical method. The horizontal micro-section of the apparent resistivity in the limestone layer is shown in Fig. 9. Notably, the low-resistivity region DZ1 is close to the roadway. The abscissa is from 200 to 250 m, and the ordinate is from 90 to 160 m. The value of the apparent resistivity is very low. The differences in the electrical properties between the coal seams are comparatively small, indicating that the water-bearing capacity in this region is low. A comparison of Figs. 4 and 9 shows that the region of abnormality was diminished and the apparent resistivity increased, indicating that the grouting was effective.

Conclusions

Using the network parallel electrical method, we investigated the properties of the floor of working face no. II 632 at the Hengyuan coal mine. An abnormal region of low resistivity, also known as the abnormal water-bearing region, was mainly caused by activation of fault DF137 during mining.

Based on the limit equilibrium and Mohr–Coulomb theories, we established a formula to determine the critical water pressure that would cause an inrush when mining near faults. By substituting the parameters of fault DF137 into this formula, we determined that mining at working face DF137 would activate fault DF137 and lead to water inrush.

Using the FSI method in Flac3D, the pathway of water inrush around fault DF137 was identified and simulated under the coupled pressures of confined water and those

induced by mining. As the working face advances, the confined water will flow upward along the fault. When the working face is 15 m from the fault, the confined water will rush along the floor and into the working face. To prevent water inrush, we suggested grouting the floor of the working face. This was done, and based on the geophysical results, we found that the abnormal water-bearing region shrank after grouting, indicating that the grouting was effective.

Acknowledgements This study was supported by the National Natural Science Foundation of China (No. 5140413), the special Subject Grant of National “973” Basic Research program of China (No. 2015CB251602), the Open Projects of State Key Laboratory For Geomechanics and Deep underground Engineering (No. SKL-GDUEK1212), the Natural Science Foundation of Anhui Province (No. 1508085ME77), the Major Research Funding Project of Natural Science of Anhui Province University (No. KJ2018ZD010), and the National Science Technology Major (No. 2016X05043).

References

- Guo BH, Cheng T, Wang L (2017) Physical simulation of water inrush through the mine floor from a confined aquifer. *Mine Water Environ*. <https://doi.org/10.1007/s10230-017-0488-7>
- Hofmann GF, Scheepers LJ (2011) Simulating fault slip areas of mining induced seismic tremors using static boundary element numerical modelling. *Mining Technol* 120(1):53–64
- Hu XY, Wang LG, Lu YL, Yu M (2014) Analysis of insidious fault activation and water inrush from the mining floor. *J Chin Univ Min Technol* 24(4):477–483
- Lee D, Yim G-J, Ji S-W, Cheong Y-W (2012) Study on distribution characteristics of some water parameters properties of mine drainage in an oxidation pond, Hwangji–Yuchang coal mine, South Korea. *Environ Earth Sci*. <https://doi.org/10.1007/s12665-012-1735-7>
- Li LC, Yang TH, Liang ZZ, Zhu WC, Tang CA (2011) Numerical investigation of groundwater outbursts near faults in underground coal mines. *Int J Coal Geol* 85(3–4):276–288
- Li SC, Zhou ZQ, Li LP et al (2013) Risk assessment of water inrush in karst tunnels based on attribute synthetic evaluation system. *Tunn Undergr Space Technol* 38:50–58
- Li WP, Liu Y, Qiao W et al (2017) An improved vulnerability assessment model for floor water bursting from a confined aquifer based on the water inrush coefficient method. *Mine Water Environ*. <https://doi.org/10.1007/s10230-017-0463-3>
- Liu PG, Tao YZ, Shang MT, Yao M (2014) The calculation of mine water yield using the non-continuous flow theory. *Environ Earth Sci* 71:975–981. <https://doi.org/10.1007/s12665-013-2592-8>
- Liu SL, Liu WT, Yin DW (2017) Numerical simulation of the lagging water inrush process from insidious fault in coal seam floor. *Geotechnol Geol Eng* 35:1013–1021. <https://doi.org/10.1007/s10706-016-0156-x>
- Miao XX (2011) Method and practice of water preserved coal mining in arid and semi arid mining area. China Univ of Mining and Technology Press, Xuzhou (in Chinese)
- Sun J, Wang LG, Hu Y (2019) Mechanical criteria and sensitivity analysis of water inrush through a mining fault above confined aquifers. *Arab J Geosci* 12(1):4
- SACMSC (State Administration of Coal Mine Safety of China) (2009) Interpretation of the regulations of mine water disaster prevention. China Univ of Mining and Technology Press, Xuzhou, pp 227–236 (in Chinese)

- Sainoki A, Hani SM (2014) Dynamic behaviour of mining-induced fault slip. *Int J Rock Mech Min Sci* 66(1):19–29
- Wang XY, Wang TT, Wang Q, Liu XM, Li RZ, Liu BJ (2017) Evaluation of floor water inrush based on fractal theory and an improved analytic hierarchy process. *Mine Water Environ* 36:87–95
- Wu Q, Guo X, Shen J, Xu S, Liu S, Zeng Y (2017) Risk assessment of water inrush from aquifers underlying the Gushuyuan coal mine, China. *Mine Water Environ* 36(1):96–103. <https://doi.org/10.1007/s10230-016-0410-8>
- Xu JP, Liu SD, Wang B, Zhang P, Gui H (2012) Electrical monitoring criterion for water flow in faults activated by mining. *Mine Water Environ* 31:172–178
- Yin SX, HU WY (2008) Study on water blocking performance and natural lift height of rock strata. *Coal Geol Explor* 36(1):34–36 (in Chinese)
- Zhang R, Jiang ZQ, Zhou HY, Yang CW, Xiao SJ (2014) Groundwater outbursts from faults above a confined aquifer in the coal mining. *Nat Hazards* 71(3):1861–1872
- Zhao Y, Li PF, Tian SM (2013) Prevention and treatment technologies of railway tunnel water inrush and mud gushing in China. *J Rock Mech Geotech Eng* 5(6):468–477
- Zhou QL, Juan H, Arturo H (2017) The numerical analysis of fault-induced mine water inrush using the extended finite element method and fracture mechanics. *Mine Water Environ*. <https://doi.org/10.1007/s10230-017-0461-5>